Quantifying thermal transport in amorphous silicon using mean free path spectroscopy

Ying Pan,[1,*] Jiawei Zhou,[2,*] and Gang Chen[2,†]

[1]*Department of Materials Science and Engineering, Massachusetts Institute of Technology, Cambridge, Massachusetts 02139, USA*

[2]*Department of Mechanical Engineering, Massachusetts Institute of Technology, Cambridge, Massachusetts 02139, USA*

(Received 16 August 2019; revised manuscript received 11 February 2020; accepted 20 March 2020; published 15 April 2020)

The wide application of amorphous materials in solar cells, memristors, and optical sensors has stimulated interest in understanding heat conduction in amorphous systems owing to their thermal management issues. Thermal transport in amorphous materials fundamentally differs from their crystalline counterparts due to the lack of long-range order. Despite great progress in understanding the thermal transport in crystalline materials over the past few decades from both first-principles computations and thermal transport characterizations, details of heat conduction in amorphous systems remain largely unknown. Here, we quantify different types of heat carriers in amorphous silicon using mean free path spectroscopy, with characteristic sizes down to 50 nm. We show that despite its disordered nature, more than half of thermal conductivity is contributed by propagating vibrational waves, which have mean free paths mostly above 100 nm. This provides direct evidence supporting the diversity of heat carriers in amorphous systems; some modes transport heat as propagating waves, while others do not. Our results suggest mean free path spectroscopy is a versatile tool for understanding thermal transport in disordered systems.

DOI: 10.1103/PhysRevB.101.144203

I. INTRODUCTION

Recent decades have witnessed wide applications of amorphous materials in microelectronic and energy conversion devices, such as solar cells [1], memristors [2], infrared sensors [3], and transistors [4]. As thermal management is critical to device performance, the thermal transport behavior in amorphous systems has received increasing attention recently [5–14]. In crystalline solids, the heat carriers are quantized lattice vibrations with well-defined wave vectors, known as phonons [15]. In amorphous materials, however, the absence of long-range order leads to the breakdown of the phonon picture. Instead, a variety of vibrational modes are allowed that can carry heat, including modes behaving as propagating waves, known as "propagons" (similar to phonons but without a well-defined wave vector) [16,17], or nonpropagating modes that exhibit random vibrations, such as "diffusons" (extended in space) and "locons" (localized in space) [18]. Because the thermal transport involves such a broad range of heat carriers, quantifying the contributions from different heat carriers has become a central topic in understanding the materials' heat conduction behavior [19–21].

Spectroscopy methods such as neutron or Raman scattering have been widely used to categorize the vibrational modes in crystalline and molecular materials. For amorphous systems, the lack of long-range order allows the scattering process to occur from almost all the vibrational modes, and consequently, spectroscopy tools in general reflect the vibrational density of states but cannot distinguish their difference for thermal transport [22–24]. Alternatively, transport measurements on amorphous samples have been conducted to investigate the size effect in thermal conductivity, using the classical electrical resistance thermometer [25,26], the 3ω method [7,27], thermoreflectance [8,28], and the thermal-bridge method [9]. The size effect occurs when modes with long propagating lengths experience strong scatterings by sample boundaries. While these experiments have shown a strong size effect and suggested propagating modes may contribute significantly to the total thermal conductivity [7–9,28], the methods are indirect as the thermal transport is inferred mostly based on samples prepared with different thicknesses, subject to the uncertainty due to sample variations. The lack of an experimental tool to quantify the contributions of propagating and nonpropagating modes in a single sample has impeded efforts to understand thermal transport in amorphous material-based nanostructures, where the sample-specific structures may have a large impact on their transport properties [7].

The distinction between propagating and nonpropagating modes is given by the Ioffe-Regel criterion [18], which states that the propagating length for propagons is larger than their quantum wavelength and thus mean free paths (MFPs) are well defined, while for nonpropagating modes MFPs become smaller than their wavelength and are no longer meaningful. Consequently, the mean free path spectroscopy [19], recently developed for understanding nanoscale thermal transport in crystalline materials, presents an ideal tool to quantify different types of heat carriers in an amorphous material. For crystalline materials, Dames and Chen [29,30] introduced cumulative thermal conductivity to describe the broad phonon spectrum based on their mean free paths,

$$F(\Lambda_{\mathrm{m}}) = \int_0^{\Lambda_{\mathrm{m}}} \frac{1}{3} C v \Lambda \left(-\frac{d\Lambda}{d\omega} \right)^{-1} d\Lambda \qquad (1)$$

*These authors contributed equally to this work.
†Corresponding author: gchen2@mit.edu

where C, v, and Λ are the phonon mode-specific heat capacity, group velocity, and mean free path. Recent developments in first-principles computations and mean free path spectroscopy techniques have allowed quantification of the cumulative thermal conductivity and thus the broad mean free path spectrum in crystalline material systems including alloys with certain disorder [19–21,31–33]. In contrast, the mean free path spectrum for the propagating modes in disordered systems and their relative contribution compared to nonpropagating modes remain largely unknown. In this work we present a comparative study of the thermal transport in amorphous silicon (a-Si) and crystalline silicon (c-Si) with mean free path spectroscopy by probing the quasiballistic thermal transport with varying heater sizes using the time-domain thermoreflectance method. Aluminum metal grating with linewidths down to 50 nm allows us to extract the mean free path spectrum of phonons (propagons in the case of a-Si). Furthermore, we provide a quantitative measure of the relative contribution to heat conduction in a-Si from different heat carriers, with more than half the contribution to the total thermal conductivity coming from the propagating modes.

II. EXPERIMENTAL DETAILS

A. Principle of mean free path spectroscopy

Quasiballistic heat conduction occurs when the characteristic lengths of heat sources are comparable to the mean free paths of propagating heat carriers [34]. By varying this characteristic length, one can thus probe the mean free path spectrum of propagating modes contributing to heat conduction [19,33,35]. In our experiments, one-dimensional metal gratings with width w are used as nanoscale heaters, as illustrated in Fig. 1. Figure 1(a) shows the diffusive limit ($w \gg \Lambda$) scenario, where heat carriers experience strong scatterings and reach thermal equilibrium. In this case the thermal decay from the heat sources can be well described by a diffusion equation with the bulk thermal conductivity κ_{bulk}. When the size of the heater is comparable to or smaller than Λ, part of the heat carriers will propagate ballistically from the heater to the underlying substrate. By gradually reducing the characteristic length w of heaters [Fig. 1(b)], the measured thermal conductivity thus represents the contribution to the thermal transport from different portions of the entire spectrum of heat carriers [19,33,35].

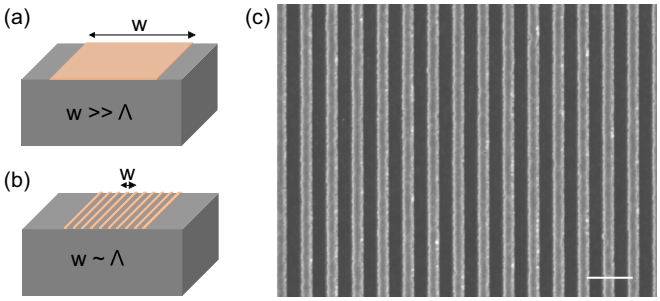

FIG. 1. Illustration of diffusive and quasiballistic phonon transport. (a) In the diffusive limit, $w \gg \Lambda$, phonons experience enough scattering and reach thermal equilibrium. Measured thermal conductivity corresponds to the bulk thermal conductivity of the substrate material. (b) As the characteristic length w is smaller than Λ, phonons propagate ballistically from the heater to the substrate. (c) Scanning electron microscopy image of a typical aluminum grating on a-Si sample substrate. The scale bar is 500 nm.

B. Sample preparation and characterization

The samples include an a-Si film ($\sim$1.2 μm thick) and a crystalline silicon. The a-Si film is deposited by low-pressure chemical vapor deposition (LPCVD) on a crystal silicon substrate. First, the sample is loaded vertically with its face perpendicular to the axis of the chamber tube. The silane (SiH_4) gas is then turned on to flow into the chamber at a constant flow rate of 30 sccm. The deposition conditions are maintained at 550 °C in temperature and 250 mTorr in pressure. The deposition rate is approximately 5 nm/min.

It is important to characterize the structure of amorphous materials when comparing different studies because the degree of disorder could be different depending on the sample preparation. To this end, we have used Raman spectroscopy measurements to characterize the structure of the LPCVD-grown a-Si. Compared to the c-Si, which has a sharp Raman peak around 520 cm^{-1} that comes from its optical phonon mode, a much broader peak is found in a-Si around 480 cm^{-1} [Fig. S3(a)]. Following Beeman *et al.* [36], we define the linewidth Γ of this broad peak as twice the half width on the high-frequency side at half the maximum height, which gives $\Gamma = 65$ cm^{-1}. It has been understood that this line broadening effect comes as a result of the local disorder of the Si-Si bond that deviates from the ideal tetrahedral configuration. One quantity that describes this disorder is the rms bond-angle distortion $\Delta\theta_b$ (zero in the case of crystalline silicon). Based on the Beeman-Tsu-Thorpe model, our measured linewidth corresponds to a rms bond-angle distortion of $\Delta\theta_b \approx 8.3°$. This value is on the low end of bond-angle distortions [36]. Furthermore, a Raman spectrum around 2000 cm^{-1} shows that the sample does not have any peak [Fig. S3(b)]. It is known that if the sample is hydrogenated, Si-H bonds would lead to Raman peaks in this spectral range [37]. These results signal that the a-Si sample is not hydrogenated and has a low degree of bond-angle disorder.

After obtaining the a-Si film together with the crystalline silicon as the reference material, we then fabricated metal grating lines onto both of these samples. The nanofabrication procedure is based on a metal liftoff method. Details of the fabrication procedure are provided in the Supplemental Material (SM) [38]. Figure 1(c) shows a typical scanning electron microscopy image of the fabricated metal gratings. The aluminum grating width varies from 400 to 50 nm, and the spacing between adjacent lines is fixed at 150 nm.

C. Thermal conductivity measurement

The thermal conductivity of samples was measured using a polarized two-tint time domain thermoreflectance (TDTR) setup (see Ref. [21] for more details). In the TDTR method [39–41], a pump laser first heats up the sample, and as the heat decays into the substrate, a second probe beam is reflected from the sample surface; meanwhile, the signal is recorded as

a function of the delay time. As the reflectance changes with temperature, the signal thus monitors the surface temperature decay, from which the substrate thermal conductivity can be extracted. It is worth noting that the thermal decay as characterized by the peak temperature of the heater is different from that in the transient grating experiments (by either crossing of two beams or diffraction from metallic gratings) which measure the temperature difference between the peak and valley of the grating [35]. A metal layer is typically deposited onto the sample to avoid direct heating of the sample and for a larger thermoreflectance response. Aluminum was chosen due to its high thermoreflectance coefficient at our probe laser wavelength (∼785 nm) [42].

For TDTR measurements on samples with grating structure, it is necessary that most of the laser energy does not transmit through the metal layer and generates electron-hole pairs that influence the signal. First, a polarizer is added, with its polarization direction parallel to the grating lines, which enhances the absorption of the pump and probe by the grating structure so that the transmission is reduced. Furthermore, we have adopted a two-tint configuration, where long-pass and short-pass filters confine the pump and probe wavelengths to 780 and 790 nm, respectively. As the spacing (the gap between adjacent lines) is fixed at 150 nm, the pump and probe beams with the wavelength at ∼785 nm will have minimal transmission due to their larger wavelength compared to the spacing.

The optical simulation for aluminum metal grating on *c*-Si and *a*-Si shows that less than 10% of the total energy of incoming light will transmit through the metal grating. We have also experimentally verified the insignificant laser transmittance by varying the polarization angle relative to the grating lines (the details of the modeling and experiment can be found in Sec. S3 in the SM). The polarizer together with the two-tint configuration thus avoids direct substrate heating from the laser, as was verified by Zeng *et al.* in our previous work [21]. Furthermore, based on the simulated optical absorption and ignoring the metal layer, we estimate the steady-state temperature rise for the pump and probe beams to be, at most, 26° and 8°, respectively (SM, Sec. S4). While there is a modest temperature rise in our system, we note that the thermal properties of the measured samples (*c*-Si and *a*-Si) have small changes within such a temperature range [5].

III. RESULTS AND DISCUSSIONS

A. Size-dependent thermal conductivity

We measured the effective thermal conductivity of amorphous silicon with various characteristic lengths w (metal linewidth) at room temperature, as shown in Fig. 2. Figure 2(a) shows plots of phase versus delay time for *a*-Si with several representative grating widths. The data can be fitted using an effective thermal conductivity based on a diffusive transport model. The interface is treated as a thermal resistance and included in our fitting model. This treatment is acceptable in our system for the following reasons. First, while for the metal/nonmetal interface studies have proposed electron-phonon coupling across the interface as an additional heat

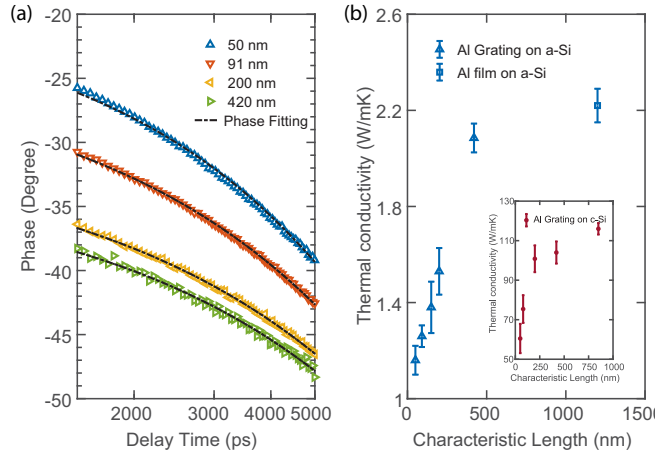

FIG. 2. TDTR experiments reveal a characteristic length-dependent thermal conductivity in *a*-Si. (a) Measured phase versus delay time for *a*-Si with aluminum grating and the fitting result using an effective thermal conductivity based on a diffusive transport model. (b) Effective thermal conductivity changes with respect to the characteristic length w in *a*-Si. For *a*-Si with aluminum grating the characteristic length is the metal linewidth, while for the aluminum film this length represents the thickness of the *a*-Si sample. The inset shows measured thermal conductivity of the crystalline silicon sample. The uncertainty is calculated based on the standard deviation of the measurement results.

transfer channel [43–45], from simulation it is found that for the Al/*c*-Si interface phonon-phonon coupling is dominant and the spatial span of the nonequilibrium region near the interface is usually small [46]. Moreover, compared to phonons in *c*-Si, vibrational modes in *a*-Si at a similar frequency level have much smaller propagating lengths [13]. The above observations suggest that the spatial span of the nonequilibrium region near the Al/*a*-Si interface is small, such that the thermal transport across the interface can be treated as an effective interfacial resistance. By fitting the thermoreflectance data we extract the interfacial thermal resistance and effective thermal conductivity at different grating widths. The fitted thermal interface conductance shows no apparent size dependence (SM, Fig. S7), consistent with previous experiments [19,21] as well as heat transport modeling [47] that explicitly includes the phonon transmittance across the interface. From the variation of the effective thermal conductivity with the grating width we then infer the nondiffusive thermal transport from the nanoscale heaters to the sample substrate. Figure 2(b) shows the fitted effective thermal conductivity of silicon with varying characteristic lengths averaged between two modulation frequencies. No modulation frequency dependence was observed in the samples (Fig. S6). The measured bulk thermal conductivity of *a*-Si is about 2.2 W/mK, which is in line with previously published experiments [7–9,28].

Over the past few decades, the thermal transport property of *a*-Si has been studied theoretically in detail based on lattice dynamics or molecular dynamics simulations [10,11,13,14,48,49]. The theory predicts the existence of propagating modes (propagons) with a long MFP in *a*-Si. In Fig. 2(b), *a*-Si shows strong size-dependent thermal conductivity. This result is consistent with previous measurements

on a-Si samples with different thicknesses [7–9]. One feature of our measurement is that there is still a finite contribution to the total thermal conductivity even at the smallest metal linewidth, indicating there are heat carriers that do not experience much from the size effect. These contributions are believed to come from nonpropagating modes. However, the boundary between the propagating and nonpropagating modes has been under debate. Past studies of thermal conductivity in amorphous silicon thin films (in the cross-plane direction, the same as ours) seem to suggest that the thermal conductivity does not decrease further for film thicknesses below 100 nm [8,9]. However, most of these measurements are subject to large uncertainty due to the presence of interfacial resistance and sample-to-sample variations, and therefore, the differences below 100 nm are not well resolved.

On the other hand, recent simulations suggest that propagating modes may exist with mean free paths well below 100 nm [13,49]. Although the behavior of those extended nonpropagating modes may be altered by the periodic boundary condition in the smaller computational cell, these results nonetheless suggest that the boundary between propagating and nonpropagating modes may occur at a much smaller length scale. Our measurement supports this picture by showing that the thermal conductivity does not plateau at 100 nm but slightly decreases with decreasing linewidths. The previous observation of the seemingly saturating thermal conductivity can be understood because a major portion of the propagating modes still come from those with mean free paths larger than 100 nm, as seen by the large decrease of thermal conductivity from larger linewidths down to around 100 nm. Moreover, the large uncertainty in previous reports may also mask the differences in thermal conductivity below 100 nm, as nonpropagating modes start to dominate the heat conduction. The recent study by Kwon *et al.* reached a similar conclusion by studying thermal conductivity in amorphous silicon nanotubes with different shell thicknesses but in the axial direction [9].

B. Mean free path reconstruction

The characteristic length-dependent thermal conductivity allows us to reconstruct the cumulative thermal conductivity, which provides a quantitative description of the mean free path spectrum. For this we have also measured the single-crystalline silicon as a benchmark material so that a comparative study can be performed. Figure 3(a) shows the normalized thermal conductivity as a function of metal linewidths for both c-Si and a-Si. Below we use the same reconstruction scheme for both samples, effectively treating propagons in amorphous silicon the same as phonons.

The reduction of thermal conductivity with decreasing heater sizes can be described by a suppression function S, which in our case of metal grating heaters depends on both the ratio between the mean free path and linewidth and the filling fraction [21]:

$$\kappa = \int_0^\infty S\left(\frac{\Lambda}{w}, \frac{w}{L}\right) f_p(\Lambda) d\Lambda + \kappa_{np}, \tag{2}$$

where f_p is the differential thermal conductivity at a given mean free path from propagating modes and κ_{np} is the

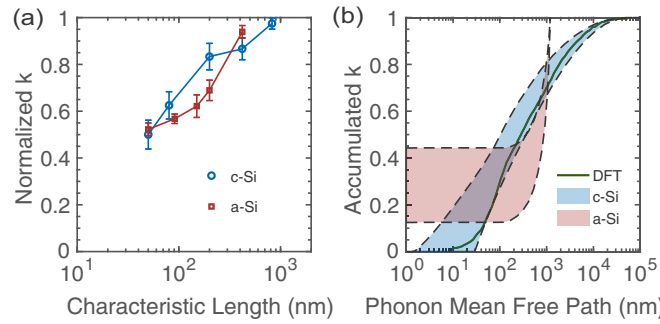

FIG. 3. Thermal conductivities of c-Si and a-Si. (a) Normalized thermal conductivity (to their bulk value) with respect to the characteristic length. (b) Cumulative thermal conductivity. The olive green line represents the density functional theory calculation result [32].

contribution from nonpropagating modes. The suppression function quantifies how the contribution to heat flux from heat carriers with certain MFPs is suppressed with respect to the Fourier's law prediction. The key assumption is that the suppression function depends on only the experimental heating geometry, while the material properties influence the measurement through the MFP distribution f_p. In such a case, the same suppression function can be found in a model "gray-body" material and can be calculated by solving the gray-body Boltzmann transport equation (BTE) [47]. Briefly, we solve the transient heat diffusion in the corresponding heating geometry using the phonon Boltzmann transport equation assuming all phonons have the same mean free paths (gray-body assumption). Here, the gray-body assumption is used only for obtaining the suppression function at different length scales. The MFP reconstruction from the experimental data, which will be shown later, still considers the entire MFP distribution. For the simulation, an initial temperature rise is applied at the metal grating and drives the heat flow into the substrate. The free boundaries are modeled assuming specular reflection, and the boundary condition treatment (diffusive or specular) is found to have a minimal impact on the simulation results [47]. For a given grating width and filling fraction, the surface temperature rise is monitored and fitted with Fourier's diffusion equation to yield an effective thermal conductivity. By varying the grating width and filling fraction, a suppression function with respect to the two nondimensional numbers ($\frac{\Lambda}{w}$ and $\frac{w}{L}$) can be obtained.

With the suppression function, Eq. (2) can then be rewritten to infer the cumulative thermal conductivity by taking the derivative of the suppression function, denoted as the kernel function K (see the derivation in the SM),

$$\kappa = S^\infty + \int_0^\infty K\left(\frac{\Lambda}{w}, \frac{w}{L}\right) \frac{1}{L} F(\Lambda) d\Lambda, \tag{3}$$

where S^∞ is the value of the suppression function at an infinitely large mean free path, which arises from the overlapping of ballistic transport between adjacent grating lines [47], and F, the cumulative thermal conductivity, takes into account the contributions from both propagating and nonpropagating modes. The suppression and kernel functions in general depend on the heating geometry and can be computed separately using Monte Carlo methods [47].

To reconstruct the cumulative thermal conductivity $F(\Lambda)$, we need to solve the inverse problem given by Eq. (3). Such an inverse problem often does not have a unique solution, and Minnich proposed an optimization procedure to reconstruct the function F with certain constraints [50]. For amorphous materials, our *a priori* assumptions for F are (1) the cumulative curve goes from a positive finite value to 1, namely, $F(0) \geqslant 0$ and $F(\infty) = 1$; (2) F should be monotonically increasing; and (3) F is smooth. The first condition is different from previous work in that we do not require F to start from zero. This is because in amorphous materials there are nonpropagating modes which do not experience an appreciable size effect. Therefore, there could be a significant contribution to the thermal conductivity even at the smallest heater size. The last condition comes from the observation that most cumulative thermal conductivities are averaged over a broad phonon spectrum and seldom have sharp features. We further note that because our *a*-Si film thickness is 1200 nm, boundary scatterings limit the maximum mean free path of propagating modes in *a*-Si to approximately 1200 nm, and for *a*-Si we reconstruct F only up to this length scale.

Figure 3(b) shows the reconstructed cumulative thermal conductivity for crystalline and amorphous silicon with a credible interval constructed based on the uncertainty in the measurements (SM, mean free path reconstruction). The reconstructed phonon MFP spectrum for crystalline silicon is consistent with previous first-principles calculations which show that phonon MFPs in *c*-Si span a broad range from 10 nm to a few micrometers [32,51]. In comparison, while a strong size effect has also been seen in *a*-Si, the propagating modes that are subject to the size effect have mean free paths mostly above 100 nm. This result indicates that while propagating modes with MFPs smaller than 100 nm exist, their contribution to the total thermal conductivity is small compared to those with longer MFPs, which is in agreement with previous work [8,9]. The reconstructed cumulative thermal conductivity has a larger uncertainty than the measured thermal conductivity values due to the nonuniqueness of solving the inverse problem. Nevertheless, the reconstructed cumulative curve shows that propagons contribute significantly (about 70%) to the total thermal conductivity in our *a*-Si sample. Due to the finite sample size, propagating modes experience strong boundary scatterings. One expects that in an intrinsic amorphous silicon sample without boundaries the relative contribution from propagating modes could be even larger. In comparison, the nonpropagating modes contribute to the rest about 30% of the thermal transport. Because the nonpropagating modes do not have well-defined mean free paths, they diffuse on a length scale comparable to their wavelength. Correspondingly, their contribution to the thermal transport will be minimally affected by the shrinking heater size, as shown by the plateau in the cumulative curve at the small mean free path limit. We further note that while *a*-Si and *c*-Si have comparable covalent bonds, the mean free path spectrum of propagons in *a*-Si does not necessarily overlap with that of phonons in *c*-Si due to the different scattering mechanisms. As pointed out by Moon *et al.*, propagating modes in amorphous silicon may also experience scatterings from the fluctuations of the elastic modulus, which alters their transport behavior compared to phonons in *c*-Si [13].

IV. CONCLUSION

In this work, the TDTR technique with varying heater size was used to study the thermal transport in crystalline and amorphous silicon. By reconstructing the mean free path cumulative thermal conductivity, it was shown that different types of heat carriers, both propagating and nonpropagating, can contribute to the thermal transport in an amorphous system, distinct from the heat conduction in crystalline materials where heat is mainly carried by propagating phonons. We directly quantified the contributions from these different heat carriers, with propagating modes, known as propagons, contributing to more than half of the total thermal conductivity and having relatively long mean free paths. This result supports the existence of long mean free path modes in disordered materials. The rest of the thermal transport is contributed by nonpropagating modes that do not experience a strong size effect. With the ability to fabricate nanostructures with further reduced dimensions, the mean free path spectroscopy can potentially be applied to other disordered materials to study their thermal transport and the contributions from different vibrational modes.

ACKNOWLEDGMENTS

The authors thank Prof. J. Hu at the Department of Materials Science and Engineering at MIT for helpful discussions. We also thank Dr. L. Zeng, Dr. K. Chen, and Dr. A. J. Schmidt for advice on the experimental setup. This work was supported by the DARPA MATRIX program, under Grant No. HR0011-16-2-0041. The experimental work was carried out at the Center for Nanoscale Systems (CNS) clean room at Harvard University. The measurement work was carried out at the Rohsenow Kendall Heat Transfer Laboratory at MIT.

[1] D. E. Carlson and C. R. Wronski, Amorphous silicon solar cell, Appl. Phys. Lett. **28**, 671 (1976).

[2] Z. Q. Wang, H. Y. Xu, X. H. Li, H. Yu, Y. C. Liu, and X. J. Zhu, Synaptic learning and memory functions achieved using oxygen ion migration/diffusion in an amorphous InGaZnO memristor, Adv. Funct. Mater. **22**, 2759 (2012).

[3] R. Street, *Technology and Applications of Amorphous Silicon* (Springer, Berlin, 2000).

[4] M. J. Powell, The physics of amorphous-silicon thin-film transistors, IEEE Trans. Electron Devices **36**, 2753 (1989).

[5] B. L. Zink, R. Pietri, and F. Hellman, Thermal Conductivity and Specific Heat of Thin-Film Amorphous Silicon, Phys. Rev. Lett. **96**, 055902 (2006).

[6] S. Moon, M. Hatano, M. Lee, and C. P. Grigoropoulos, Thermal conductivity of amorphous silicon thin films, Int. J. Heat Mass Transfer **45**, 2439 (2002).

[7] X. Liu, J. L. Feldman, D. G. Cahill, R. S. Crandall, N. Bernstein, D. M. Photiadis, M. J. Mehl, and D. A. Papaconstantopoulos, High Thermal Conductivity of a Hydrogenated Amorphous Silicon Film, Phys. Rev. Lett. **102**, 035901 (2009).

[8] J. L. Braun, C. H. Baker, A. Giri, M. Elahi, K. Artyushkova, T. E. Beechem, P. M. Norris, Z. C. Leseman, J. T. Gaskins, and P. E. Hopkins, Size effects on the thermal conductivity of amorphous silicon thin films, Phys. Rev. B **93**, 140201 (2016).

[9] S. Kwon, J. Zheng, M. C. Wingert, S. Cui, and R. Chen, Unusually high and anisotropic thermal conductivity in amorphous silicon nanostructures, ACS Nano **11**, 2470 (2017).

[10] Y. He, D. Donadio, and G. Galli, Heat transport in amorphous silicon: Interplay between morphology and disorder, Appl. Phys. Lett. **98**, 144101 (2011).

[11] J. M. Larkin and A. J. H. McGaughey, Thermal conductivity accumulation in amorphous silica and amorphous silicon, Phys. Rev. B **89**, 144303 (2014).

[12] W. Lv and A. Henry, Examining the validity of the phonon gas model in amorphous materials, Sci. Rep. **6**, 37675 (2016).

[13] J. Moon, B. Latour, and A. J. Minnich, Propagating elastic vibrations dominate thermal conduction in amorphous silicon, Phys. Rev. B **97**, 024201 (2018).

[14] T. Zhu and E. Ertekin, Generalized Debye-Peierls/Allen-Feldman model for the lattice thermal conductivity of low-dimensional and disordered materials, Phys. Rev. B **93**, 155414 (2016).

[15] J. M. Ziman, *Electrons and Phonons* (Oxford University Press, London, 1960).

[16] P. B. Allen and J. L. Feldman, Thermal conductivity of disordered harmonic solids, Phys. Rev. B **48**, 12581 (1993).

[17] P. Sheng and M. Zhou, Heat conductivity of amorphous solids: Simulation results on model structures, Science **253**, 539 (1991).

[18] P. B. Allen, J. L. Feldman, J. Fabian, and F. Wooten, Diffusons, locons and propagons: Character of atomic vibrations in amorphous Si, Philos. Mag. B **79**, 1715 (1999).

[19] A. J. Minnich, J. A. Johnson, A. J. Schmidt, K. Esfarjani, M. S. Dresselhaus, K. A. Nelson, and G. Chen, Thermal Conductivity Spectroscopy Technique to Measure Phonon Mean Free Paths, Phys. Rev. Lett. **107**, 095901 (2011).

[20] Y. Hu, L. Zeng, A. Minnich, S. Dresselhaus, and G. Chen, Spectral mapping of thermal conductivity through nanoscale ballistic transport, Nat. Nanotechnol. **10**, 701 (2015).

[21] L. Zeng, K. C. Collins, Y. Hu, A. A. Maznev, S. Huberman, V. Chiloyan, J. Zhou, X. Huang, K. A. Nelson, and G. Chen, Measuring phonon mean free path distributions by probing quasiballistic phonon transport in grating nanostructures, Sci. Rep. **5**, 17131 (2015).

[22] R. Shuker and R. W. Gammon, Raman-Scattering Selection-Rule Breaking and the Density of States in Amorphous Materials, Phys. Rev. Lett. **25**, 222 (1970).

[23] J. E. Smith, M. H. Brodsky, B. L. Crowder, M. I. Nathan, and A. Pinczuk, Raman Spectra of Amorphous Si and Related Tetrahedrally Bonded Semiconductors, Phys. Rev. Lett. **26**, 642 (1971).

[24] U. Buchenau, Inelastic neutron scattering from low-frequency vibrational excitations in amorphous solids, Z. Phys. B **58**, 181 (1985).

[25] H. Wada and T. Kamijoh, Thermal conductivity of amorphous silicon, Jpn. J. Appl. Phys. **35**, L648 (1996).

[26] S. Uma, A. D. McConnell, M. Asheghi, K. Kurabayashi, and K. E. Goodson, Temperature-dependent thermal conductivity of undoped polycrystalline silicon layers, Int. J. Thermophys. **22**, 605 (2001).

[27] D. G. Cahill, H. E. Fischer, T. Klitsner, E. T. Swartz, and R. O. Pohl, Thermal conductivity of thin films: Measurements and understanding, J. Vac. Sci. Technol. A **7**, 1259 (1989).

[28] K. T. Regner, D. P. Sellan, Z. Su, C. H. Amon, A. J. H. McGaughey, and J. A. Malen, Broadband phonon mean free path contributions to thermal conductivity measured using frequency domain thermoreflectance, Nat. Commun. **4**, 1640 (2013).

[29] C. Dames and G. Chen, *Thermoelectrics Handbook, Macro to Nano* (CRC Press, Boca Raton, 2006).

[30] F. Yang and C. Dames, Mean free path spectra as a tool to understand thermal conductivity in bulk and nanostructures, Phys. Rev. B **87**, 035437 (2013).

[31] D. A. Broido, M. Malorny, G. Birner, N. Mingo, and D. A. Stewart, Intrinsic lattice thermal conductivity of semiconductors from first principles, Appl. Phys. Lett. **91**, 231922 (2007).

[32] K. Esfarjani, G. Chen, and H. T. Stokes, Heat transport in silicon from first-principles calculations, Phys. Rev. B **84**, 085204 (2011).

[33] J. A. Johnson, A. A. Maznev, J. Cuffe, J. K. Eliason, A. J. Minnich, T. Kehoe, C. M. Sotomayor Torres, G. Chen, and K. A. Nelson, Direct Measurement of Room-Temperature Nondiffusive Thermal Transport over Micron Distances in a Silicon Membrane, Phys. Rev. Lett. **110**, 025901 (2013).

[34] G. Chen, *Nanoscale Energy Transport and Conversion: A Parallel Treatment of Electrons, Molecules, Phonons, and Photons* (Oxford University Press, Oxford, 2005).

[35] M. E. Siemens, Q. Li, R. Yang, K. A. Nelson, E. H. Anderson, M. M. Murnane, and H. C. Kapteyn, Quasi-ballistic thermal transport from nanoscale interfaces observed using ultrafast coherent soft X-ray beams, Nat. Mater. **9**, 26 (2010).

[36] D. Beeman, R. Tsu, and M. F. Thorpe, Structural information from the Raman spectrum of amorphous silicon, Phys. Rev. B **32**, 874 (1985).

[37] M. H. Brodsky, M. Cardona, and J. J. Cuomo, Infrared and Raman spectra of the silicon-hydrogen bonds in amorphous silicon prepared by glow discharge and sputtering, Phys. Rev. B **16**, 3556 (1977).

[38] See Supplemental Material at http://link.aps.org/supplemental/10.1103/PhysRevB.101.144203 for further information on the sample preparation and characterization, optical simulation of the grating structure, measurement setup and model fitting parameters, and mean free path reconstruction. The Supplemental Material includes Refs. [6,19,21,37,41,42,47,50,52–54].

[39] C. A. Paddock and G. L. Eesley, Transient thermoreflectance from thin metal films, J. Appl. Phys. **60**, 285 (1986).

[40] W. S. Capinski, H. J. Maris, T. Ruf, M. Cardona, K. Ploog, and D. S. Katzer, Thermal-conductivity measurements of GaAs/AlAs superlattices using a picosecond optical pump-and-probe technique, Phys. Rev. B **59**, 8105 (1999).

[41] D. G. Cahill, Analysis of heat flow in layered structures for time-domain thermoreflectance, Rev. Sci. Instrum. **75**, 5119 (2004).

[42] A. J. Schmidt, X. Chen, and G. Chen, Pulse accumulation, radial heat conduction, and anisotropic thermal conductivity in

pump-probe transient thermoreflectance, Rev. Sci. Instrum. **79**, 114902 (2008).

[43] M. L. Huberman and A. W. Overhauser, Electronic Kapitza conductance at a diamond-Pb interface, Phys. Rev. B **50**, 2865 (1994).

[44] A. Majumdar and P. Reddy, Role of electron-phonon coupling in thermal conductance of metal-nonmetal interfaces, Appl. Phys. Lett. **84**, 4768 (2004).

[45] G. D. Mahan, Kapitza thermal resistance between a metal and a nonmetal, Phys. Rev. B **79**, 075408 (2009).

[46] Y. N. Yang, T. Luo, K. Esfarjani, A. Henry, Z. Tian, J. Shiomi, Y. Chalopin, B. Li, and G. Chen, Thermal interface conductance between aluminum and silicon by molecular dynamics simulations, J. Comput. Theor. Nanosci. **12**, 168 (2015).

[47] L. Zeng and G. Chen, Disparate quasiballistic heat conduction regimes from periodic heat sources on a substrate, J. Appl. Phys. **116**, 064307 (2014).

[48] J. L. Feldman, M. D. Kluge, P. B. Allen, and F. Wooten, Thermal conductivity and localization in glasses: Numerical study of a model of amorphous silicon, Phys. Rev. B **48**, 12589 (1993).

[49] K. Sääskilahti, J. Oksanen, J. Tulkki, A. J. H. McGaughey, and S. Volz, Vibrational mean free paths and thermal conductivity of amorphous silicon from non-equilibrium molecular dynamics simulations, AIP Adv. **6**, 121904 (2016).

[50] A. J. Minnich, Determining Phonon Mean Free Paths from Observations of Quasiballistic Thermal Transport, Phys. Rev. Lett. **109**, 205901 (2012).

[51] A. S. Henry and G. Chen, Spectral phonon transport properties of silicon based on molecular dynamics simulations and lattice dynamics, J. Comput. Theor. Nanosci. **5**, 141 (2008).

[52] E. D. Palik, *Handbook of Optical Constants of Solids* (Academic Press, San Diego, 1985).

[53] D. T. Pierce and W. E. Spicer, Electronic structure of amorphous Si from photoemission and optical studies, Phys. Rev. B **5**, 3017 (1972).

[54] N. K. Ravichandran, H. Zhang, and A. J. Minnich, Spectrally Resolved Specular Reflections of Thermal Phonons from Atomically Rough Surfaces, Phys. Rev. X **8**, 041004 (2018).